JCTC Journal of Chemical Theory and Computation

All-Atom Calculation of the Normal Modes of Bacteriorhodopsin Using a Sliding Block Iterative Diagonalization Method

Alexey L. Kaledin,* Martina Kaledin,† and Joel M. Bowman

Department of Chemistry and Cherry L. Emerson Center for Scientific Computing, Emory University, Atlanta, Georgia 30322

Received June 22, 2005

Abstract: Conventional normal-mode analysis of molecular vibrations requires computation and storage of the Hessian matrix. For a typical biological system such storage can reach several gigabytes posing difficulties for straightforward implementation. In this work we discuss an iterative block method to carry out full diagonalization of the Hessian while only storing a few vectors in memory. The iterative approach is based on the conjugate gradient formulation of the Davidson algorithm for simultaneous optimization of L roots, where in our case $10 < L < 300$. The procedure is modified further by automatically adding a new vector into the search space for each locked (converged) root and keeping the new vector orthogonal to the eigenvectors previously determined. The higher excited states are then converged with the orthonormality constraint to the locked roots by applying a projector which is carried out using a read-rewind step done once per iteration. This allows for convergence of as many roots as desired without increasing the computer memory. The required Hessian-vector products are calculated *on the fly* as follows, $\mathbf{Kp} = d\mathbf{g}_p/dt$, where $\mathbf{K}$ is the mass weighted Hessian, and $\mathbf{g}_p$ is the gradient along $\mathbf{p}$. The method has been implemented into the TINKER suite of molecular design codes. Preliminary results are presented for the normal modes of bacteriorhodopsin (bR) up to 300 cm^{-1} and for the high frequency range between 2840 and 3680 cm^{-1}. There is evidence of a highly localized, noncollective mode at $\sim$1.4 cm^{-1}, caused by long-range interactions acting between the cytoplasmic and extracellular domains of bR.

1. Introduction

Vibrational modes of proteins are basic motions for protein dynamics and structural transitions. Normal-mode analysis (NMA) is a direct way to analyze vibrational motion.[1] This method has long been used as a tool for interpreting vibrational spectra of small molecules.[2] The frequencies obtained from NMA can be directly related to experimental infrared (IR) and/or Raman measurements. In recent years NMA has been extended to the study of large molecular systems such as proteins.[3−7] Low-frequency modes of proteins are particularly interesting, because they are related to functional properties.[8] It is believed that low-frequency collective modes are responsible for the direct flow of conformational energy in many biological processes.[9−11]

All-atom normal mode calculations of large systems are impeded by the bottleneck associated with computing and storing a full Hessian matrix.[5] An example of this is the 3.6 GB storage required for the Hessian of a system of 10 000 atoms. The use of sparse matrix techniques advocated by some authors can alleviate the storage problem significantly.[12−14] The matrix becomes sparser as the number of atoms increases, and benchmark calculations have been carried out for impressively large nanoparticles.[15] However, it is unclear to what degree the resulting eigenvalues are

* Corresponding author e-mail: akaledi@emory.edu.
† Present address: Department of Chemistry and Biochemistry, Kennesaw State University, Kennesaw, GA 30144.

10.1021/ct050161z CCC: $33.50
Published on Web 11/24/2005

corrupted by removing a large number of small matrix elements arising from the long-range interactions: electrostatic, van der Waals, etc.

Recent advances in Hessian operator techniques[16−19] have opened new possibilities for NMA of macromolecules. Pioneering work of Filippone and Parrinello[16,17] on linear response theory of Hessian demonstrated the use of direct ab initio methods combined with gradients to perform geometry optimization and iterative diagonalization of the Hessian of water dimer without explicit calculation of the Hessian matrix. Using this theory, Reiher and Neugebauer[20−23] did calculations of carbon nanotubes to determine their vibrational modes in the middle range of the spectrum. In a similar spirit, one of us later carried out calculations[24] of up to 200 lowest frequency normal modes of helium nanodroplets with the largest being a 27 000 atom system, affirming applicability of the Hessian operator theory to nanomaterials and, potentially, to biological macromolecules, the latter being the focus of the present work.

The Hessian operator method is ideally suited for combination with iterative diagonalization techniques to solve for the eigenvalues and eigenvectors of very large matrices. Basically, the resultant of Hessian multiplying on a vector is proportional to the gradient change along the vector.[16,17,25−29] This relationship follows from the harmonic expansion of the potential around a given geometry and is summarized by the following expression

$$\mathbf{Kp} = \mathrm{d}\mathbf{g}_{\mathrm{p}}/\mathrm{d}t \tag{1}$$

where $\mathbf{K}$ and $\mathbf{g}_{\mathrm{p}}$ are the mass weighted Hessian and gradient (along vector $\mathbf{p}$). The time derivative on the right-hand side is equivalent to a change over the infinitesimally short trajectory defined by $\mathbf{q} = \pm\delta t\mathbf{p}$, where $\mathbf{q}$ and $\mathbf{p}$ are the mass weighted coordinates and momenta. Thus, given a set of trial vectors spanning a small subspace, a single optimization step can be carried out by computing the residuals and evaluating the appropriate matrix elements using eq 1. The improved vectors are then used to perform another iteration, and so on, until convergence. Clearly, the storage requirement is drastically reduced: from the usual $O(N^2)$ in the conventional calculation with Hessian to $O(N)$ in the iterative calculation using eq 1, where N is the number of atoms.

In the present work we report an extension of a block Davidson iterative method,[30,31] whose modified version was tested in the earlier work,[24] by adding the capability to converge all the normal modes up to a given threshold without compromising the scaling properties of the algorithm. Benchmark calculations are presented for the normal modes of a 222 residue (3503 atoms) protein converged up to 300 cm^{-1} (a total of 1954 normal modes) and between 2840 cm^{-1} and 3680 cm^{-1} (1782 normal modes).

2. Computational Methods

To carry out full diagonalization of the matrix we combine two techniques: (1) a flexible iterative procedure and (2) a memory-efficient evaluation of matrix-vector products.

2.1. Iterative Procedure. The Hessian eigenvalue equation for normal mode I is

$$\mathbf{Ky}_I = \lambda_I\mathbf{y}_I \tag{2}$$

where $\mathbf{y}_I$ is the eigenvector with the corresponding eigenvalue λ_I. The Davidson procedure[30] for finding the lowest root ($I = 1$) of eq 2 involves optimization of a trial vector in an orthogonal subspace, a vector space that is much smaller than the size of the matrix. The approximate solution at iteration n is a linear combination of the n basis vectors, i.e.,

$$\mathbf{y}_I^{(n)} = \sum_i^n c_{Ii}^{(n)}\mathbf{b}_i \tag{3}$$

with the expansion coefficients satisfying the variational condition for the lowest root

$$\mathbf{B}^\dagger\mathbf{KB}\mathbf{c}_I^{(n)} = \lambda_I\mathbf{c}_I^{(n)} \tag{4}$$

where $\mathbf{B}$ is the column matrix of vectors $\mathbf{b}$. The new expansion vector that is added to the iterative subspace $\mathbf{B}$ is derived from perturbation theory,[30] as follows

$$\mathbf{r}_I' = -(\mathbf{D} - \lambda_I\mathbf{1})^{-1}\mathbf{r}_I'' \tag{5}$$

where $\mathbf{D}$ is the diagonal part of $\mathbf{K}$, and $\mathbf{r}_I''$ is the residual of the current approximation to the lowest root, i.e.,

$$\mathbf{r}_I'' = \mathbf{Ky}_I - \lambda_I\mathbf{y}_I \tag{6}$$

One then proceeds by appending the orthogonal complement $\tilde{\mathbf{r}}_I'$ of $\mathbf{r}_I'$ to the subspace $\mathbf{B}$ and diagonalizing the $(n + 1) \times (n + 1)$ interaction matrix $\mathbf{K_{BB}} \equiv \mathbf{B}^\dagger\mathbf{KB}$. The procedure is repeated until the eigenvalue λ_I is stationary (the eigenvalue criterion), or the norm of the residual $\mathbf{r}_I''$ is small enough (the wave function criterion). In case the number of expansions is too large, the procedure is restarted. There exist a variety of methods to improve the diagonal matrix approximation in eq 5,[32] but this discussion is beyond the scope of the present work.

The extension to excited states is straightforward and can be done by simply searching for the next lowest root subject to orthogonality constraint to all the previously converged roots. However, due to the high density of vibrational levels of macromolecules with many weak interactions, it often becomes necessary to perform a simultaneous optimization of several roots. Given a set of trial vectors $\{\mathbf{y}\}_L$ one proceeds by building up the iterative subspace $\mathbf{B}$. Each new iteration expands the subspace by L vectors, where L is the number of roots that are simultaneously optimized. This method is known as the block-Davidson method.[33] Similarly to the single root procedure, the subspace $\mathbf{B}$ is periodically collapsed to L vectors to save space.[31]

In practice, periodic collapse of the $\mathbf{B}$-space to one (or a few) vector per root hinders convergence of the Davidson procedure. Van Lenthe and Pulay[34] first demonstrated on the single root Davidson method that collapsing the $\mathbf{B}$-space on every iteration while retaining the solution vector from the previous iteration basically preserves the variational flexibility of the original method. In other words, the $\mathbf{B}$-space at iteration n consists of three vectors, namely, $\{\tilde{\mathbf{y}}_I^{(n-1)}, \mathbf{y}_I^{(n)}, \tilde{\mathbf{r}}_I^{(n)}\}$, where $\tilde{\mathbf{y}}_I^{(n-1)}$ is the orthogonal complement to $\mathbf{y}_I^{(n)}$, and

$\tilde{\mathbf{r}}_I^{(n)}$ is the *projected* orthogonal complement to $\tilde{\mathbf{y}}_I^{(n-1)}$ and $\mathbf{y}_I^{(n)}$ (cf. eq 8). This method blends together the theory of conjugate gradients and the original Davidson method for the ground state. It has also been shown that simultaneous optimization of several roots for extraction of excited states is possible in this framework.[31,35−37]

The procedure described here is a slight modification of the method suggested by Murray et al.[31] and is a straightforward adaptation of a block version of the van Lenthe−Pulay method[34] for the ground state. The next approximation to root I at iteration n is expanded in a linear combination of orthonormal **B**-space vectors

$$\mathbf{y}_I^{(n+1)} = \sum_j^{3L} c_{Ij}^{(n)}\, \mathbf{b}_j^{(n)} \tag{7}$$

$$= \sum_{j=1}^{L} c_{Ij}^{(n)}\, \mathbf{y}_j^{(n)} + \sum_{j=L+1}^{2L} c_{Ij}^{(n)}\, \tilde{\mathbf{y}}_{j-L}^{(n-1)} + \sum_{j=2L+1}^{3L} c_{Ij}^{(n)}\, \tilde{\mathbf{r}}_{j-2L}^{(n)}$$

where L is the number of roots optimized. On each iteration we solve for the expansion coefficients $\{\boldsymbol{c}_I^{(n)}\}_{3L}$ in eq 7 by diagonalizing the $3L \times 3L$ $\mathbf{K_{BB}}$ matrix. The approximation to the eigenvalue I is the corresponding eigenvalue of $\mathbf{K_{BB}}$. A similar formulation has previously been tested by Knyazev on a number of model problems in physics.[35−37]

With the constraint that the root with index J must be converged before, or simultaneously with, the root of index $J + 1$, etc., the iterations are repeated until the first l roots in the block ($1 \le l \le L$) satisfy certain convergence criteria. (The l converged vectors are then locked and appended to an existing file.) To continue with the iterative process, we use the virtual states at current and previous iteration as the guess for roots $L + 1, \cdots, L + l + 1$. These virtual states are nonoptimized eigenvectors of the $\mathbf{K_{BB}}$ matrix, i.e., $\{\boldsymbol{c}_I^{(n)}\}$, $I = L + 1, \cdots, 3L$, but, as experience shows, they provide an excellent starting point for the upper roots. The procedure does not lose its effectiveness because the virtual states share the conjugate gradient property with the L optimized vectors. The total number of converged roots, designated by a cumulative index M, is increased by l, and the index I is reset to run over the roots $M + 1, \cdots, M + L$. The following iterations simply require that the residuals $\{\mathbf{r}'_I\}_L$ be orthogonal to all the converged vectors (before adding their orthogonal complement to the iterative subspace) which is done by applying the projector to each residual

$$\mathbf{r}_I = \mathbf{r}'_I - \sum_{j=1}^{M} \mathbf{y}_j \mathbf{y}_j^{\dagger} \mathbf{r}'_I \tag{8}$$

The converged vectors $\{\mathbf{y}_I\}_M$ are read from the storage file one at a time and applied successively onto the set $\{\mathbf{r}'_I\}_L$ using eq 8; the file is then rewound to prepare for the next iteration. This read-rewind step is done once per iteration.

The upper extreme of the spectrum can be converged in the same fashion by replacing the Hessian operator with its negative, i.e., $\mathbf{K} \rightarrow -\mathbf{K}$. The eigenvalues change the sign on this transformation, while the eigenvectors are unchanged. Unlike the usual approach of designing the inverse or the shift operator,[5,12] the negative Hessian approach does not require matrix transformations or any additional matrix-vector operations. The high frequency modes are localized and converge significantly faster than the low-frequency ones. This property suggests a useful technique to first converge a bulk of the upper states and then converge the lower ones subject to orthogonality constraint.

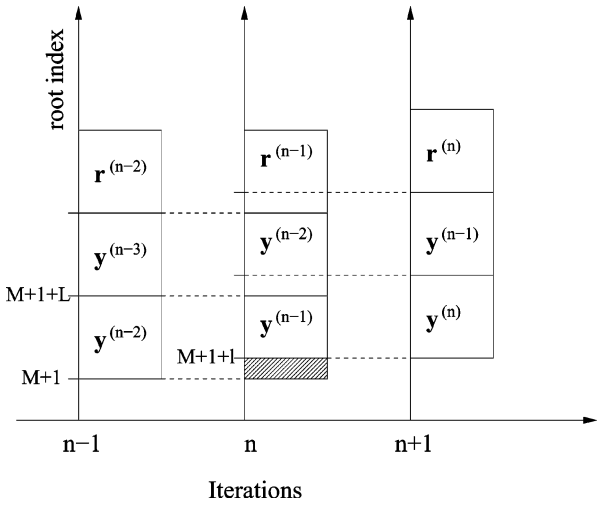

Figure 1. A schematic illustration of the iterative subspace through iterations $n - 1 \rightarrow n \rightarrow n + 1$. It is implied that the first M roots have been converged in $n - 2$ iterations. $\mathbf{y}^{(n)}$ are defined as the vectors obtained by diagonalizing the $3L \times 3L$ matrix at iteration n. In the depicted procedure, at iteration $n - 1$ no new roots have been converged. Thus, the roots $\mathbf{y}_{1,L}^{(n-1)}$, their residuals $\mathbf{r}_{1,L}^{(n-1)}$, and previous roots $\mathbf{y}_{1,L}^{(n-2)}$ are used as the updated basis for iteration n (see the dashed lines). After diagonalization, l lowest roots have been converged at iteration n (shown by the hashed space), and the corresponding vectors are passed on to the next iterations. The procedure can continue until either a frequency threshold is reached or the number of converged roots has reached the desired limit.

The method of projection by eq 8 is similar to the standard deflation techniques, and it achieves the same goal by reducing the search space.[38] However, if many eigenvectors are needed, the convergence criteria must be very strict to ensure that the cumulative error remains small. The overall procedure is stopped after M has exceeded a desired limit, or λ_M has reached a preset threshold. Figure 1 illustrates this process. The above-described procedure can be referred to as a sliding block Davidson−VanLenthe−Pulay method or simply a "sliding block" method. We note that similar iterative techniques based on the Lanczos method[39] have long existed in the literature.[35−37,40−44]

2.2. Hessian-Vector Product. Construction of the $\mathbf{K_{BB}}$ matrix requires evaluation of Hessian-vector products. Given the set of preconditioned and normalized residual vectors we must compute and store their products with the Hessian, $\{\mathbf{K}\tilde{\mathbf{r}}_I\}_L$. It can be shown analytically[16,17] that the algebraic multiplication of the $3N \times 3N$ Hessian matrix on an arbitrary vector is equivalent to differentiation of the gradient along the vector (cf. eq 1). A concise proof of this can be obtained by evaluating the time derivative of the gradient along a classical trajectory, i.e.,

$$\frac{d\mathbf{g}}{dt} = \sum_j \frac{\partial \mathbf{g}}{\partial q_j}\frac{dq_j}{dt} = \mathbf{Kp} \tag{9}$$

where **q** and **p** are the mass weighted coordinates and momenta. Since the trajectory is arbitrary, the momentum **p** can be thought of as an input (trial) vector. The time derivative is evaluated numerically by central differences. Given a unit vector, its product on the Hessian is computed as follows

$$\mathbf{K\hat{u}} = \frac{1}{2\alpha \mathbf{m}^{1/2}}[\nabla V(\mathbf{x} + \delta\mathbf{x}) - \nabla V(\mathbf{x} - \delta\mathbf{x})] \tag{10}$$

where **x** are $3N$ Cartesian coordinates, $\delta\mathbf{x} = \alpha\mathbf{m}^{-1/2}\hat{\mathbf{u}}$, $\alpha = s/(\hat{\mathbf{u}}^\dagger\mathbf{m}^{-1}\hat{\mathbf{u}})^{1/2}$, and **m** is the $3N \times 3N$ diagonal matrix of atomic masses. The displacement parameter s can be chosen in the range $10^{-5}-10^{-3}$ a_0.

2.3. Anharmonicity and Mode Lifetime. Anharmonic effects, such as mode coupling and lifetime, can be estimated directly by computing variations of the eigenvalues of the Hessian. If the normal mode vector $\mathbf{y}_I$ is sufficiently converged, the first derivative of the Hessian expectation value in mode I with respect to the normal coordinates is

$$\nabla \mathbf{y}_I^\dagger \mathbf{K} \mathbf{y}_I = \mathbf{y}_I^\dagger (\nabla \mathbf{K}) \mathbf{y}_I \tag{11}$$

The right-hand side contains the first derivative of the Hessian which carries the information of third derivatives of the potential. Similar to eq 10 the differentiation is done numerically. For the normal coordinate J

$$\left(\frac{\partial \mathbf{K}}{\partial Q_J}\right)\mathbf{y}_I = \frac{1}{2\delta Q_J}[\mathbf{K}(\mathbf{x} + \delta\mathbf{x}_J)\mathbf{y}_I - \mathbf{K}(\mathbf{x} - \delta\mathbf{x}_J)\mathbf{y}_I] \tag{12}$$

where $\delta\mathbf{x}_J$ is the Cartesian displacement vector along the normal direction J. The two Hessian vector products are then evaluated using eq 10 resulting in a total of *four* gradient computations. Using $\partial\omega_I/\partial Q_J = (\partial\lambda_I/\partial Q_J)/(2\omega_I)$ and $\delta Q_J \equiv \alpha_J$, we obtain the following expression for the derivative of the frequency

$$\frac{\partial \omega_I}{\partial Q_J} = \frac{1}{8\alpha_I\alpha_J\omega_I}\mathbf{y}_I^\dagger \mathbf{m}^{-1/2}(\nabla \mathrm{V}(\mathbf{x} + \delta\mathbf{x}_{IJ}^s) + \nabla \mathrm{V}(\mathbf{x} - \delta\mathbf{x}_{IJ}^s) - \nabla \mathrm{V}(\mathbf{x} + \delta\mathbf{x}_{IJ}^d) - \nabla \mathrm{V}(\mathbf{x} - \delta\mathbf{x}_{IJ}^d)) \tag{13}$$

where $\delta\mathbf{x}_{IJ}^{s/d} \equiv \delta\mathbf{x}_J \pm \delta\mathbf{x}_I$. For $I = J$, eq 13 provides a measure of anharmonicity of mode I, while for $I \neq J$ it yields two-mode coupling strength.

The first derivatives can be used to calculate fluctuation of frequencies and consequently the lifetime of a particular mode. The quantum mechanical expression for the variance of the frequency of normal mode I is

$$\langle \Delta\omega_I^2 \rangle = \langle \omega_I^2(\mathbf{Q}) \rangle - \langle \omega_I(\mathbf{Q}) \rangle^2 \tag{14}$$

where brackets imply a thermal average over **Q**. Using eq 13 to expand the frequency to the first order in $\delta\mathbf{Q} \equiv \mathbf{Q} - \mathbf{Q}_{eq}$ and after the cancellation of the linear and the constant terms we obtain a simplified result

$$\langle \Delta\omega_I^2 \rangle = \langle \delta\mathbf{Q}^\dagger \Omega_I \delta\mathbf{Q} \rangle \tag{15}$$

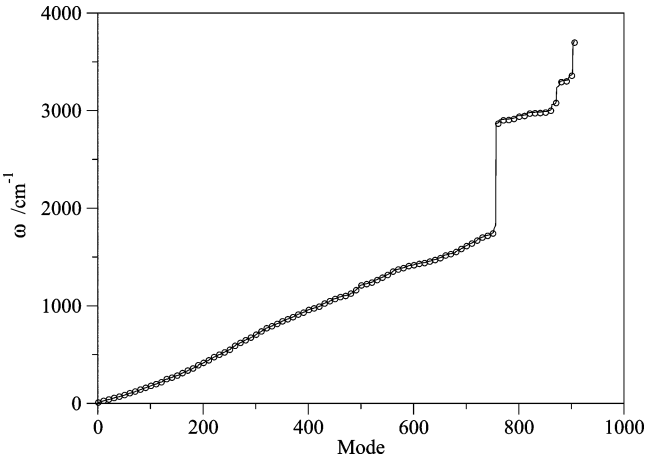

Figure 2. Frequencies of Trp-cage obtained with the block Davidson method (open circle, only every 10th frequency is show for clarity). The exact frequencies from full diagonalization (solid line) are shown for comparison.

where Ω_I is the tensor of first derivative moments, and the notation ω_I^J is short form for derivative with respect to J. The integration is completed analytically in the normal mode basis

$$\langle \Delta\omega_I^2 \rangle_{QM} = \frac{\hbar}{2}\sum_{J=1}^{M}\frac{(\omega_I^J)^2}{\omega_J}\coth\left(\frac{\hbar\omega_J}{2k_BT}\right) \tag{16}$$

The summation runs over the available normal modes. From the uncertainty principle, the lifetime of a mode can be estimated as $\tau_I \sim 1/\langle \Delta\omega_I^2 \rangle^{1/2}$. Equation 16 should provide a reliable estimate for lifetimes at low temperatures where the cubic terms in the potential dominate nonharmonic dynamics. A more rigorous theory for calculation of the lifetime involves a quantum mechanical treatment using perturbation theory,[45] as has been applied in similar calculations.[46,47]

The present method to estimate lifetime is closely related to the classical molecular dynamics and Monte Carlo simulation of the $\langle \Delta\omega^2 \rangle$ quantity, where the averaging is done over phase space classically. The corresponding classical counterpart of expression 16 in the $\hbar \rightarrow 0$ limit yields

$$\langle \Delta\omega_I^2 \rangle_{CM} = k_BT\sum_{J=1}^{M}\left(\frac{\omega_I^J}{\omega_J}\right)^2 \tag{17}$$

The results for $\langle \Delta\omega^2 \rangle$ bear close similarity to the well-known NMA expressions for atomic square fluctuations.[5]

3. Vibrational Modes of Bacteriorhodopsin

We implemented the sliding block iterative diagonalization method into the TINKER[48] suite of molecular modeling codes. The method was tested first on a small protein, Trp-cage (PDB code: 1L2Y,[49] 20 residues) for which exact normal-mode frequencies can be calculated using standard matrix diagonalization with the explicit Hessian matrix. The potential function of Trp-cage was described with the AMBER force field *ff98* for nucleic acids.[50,51] The protein was first energy minimized until the RMS gradient was less than 10^{-6} kcal/(mol Å). Figure 2 shows Trp-cage frequencies

obtained by the two methods. The two sets of eigenvectors were compared by calculating their overlap, which on average was 99.999%.

We now turn to the much larger protein, for which the calculation and storage of the full Hessian is prohibitive. Bacteriorhodopsin is a transmembrane protein found in the purple membrane of Halobacterium salinarum.[52] The study of bR has become an area of considerable interest in biochemistry seeking information about the protein's dynamics and function, for three main reasons.[53] The protein is unusually stable. It exhibits strong spectral shifts in the 400−600 nm range which are connected to reaction intermediates, and it is possible to measure vibrational spectra, characterizing geometries as well as protonated states.

The structure, dynamics, and energetics of bR have been studied extensively by molecular dynamics simulations.[54−58] Conformational modes of bR have also been studied using inelastic neutron scattering.[59,60] Recently, far-infrared (FIR) spectral measurements of wild-type (WT) and D96N mutant bR have been carried out using terahertz time domain spectroscopy.[61] In the same work,[61] the lowest few normal modes of bR were calculated using the iterative diagonalization method of Mouawad and Perahia[62] and compared to the experimental measurements. Those calculations revealed the lowest frequency mode at ∼10 cm^{-1}. Some very low-frequency modes (below 10 cm^{-1}) observed experimentally were missing in this theoretical spectrum. We noted that in this normal mode calculation[61] strict cutoffs were imposed for the nonbonded interactions.

In the present calculations, geometry optimization and the NMA were carried out in the gas phase without any cutoffs imposed on the long-range interactions. Previous studies,[63] for example, pointed out the existence of long-range interactions between the cytoplasmic and extracellular surface domains of bR that are mediated by salt bridges and hydrogen-bonded networks. Such long-range interactions are therefore expected to be of functional significance. The X-ray diffraction structure of WT-bR (PDB code: 1C3W[64]) served as the starting point for geometry optimization. The potential function was described with the Charmm27 parameter set.[65,66] The structure was energy minimized until the RMS gradient was less than 10^{-5} kcal/(mol Å). Full normal mode calculation of WT-bR would require ∼0.4 GB of memory, while the present method required a maximum of 6.3 MB. A convergence criterion of 0.001 cm^{-1} for the frequency was used for all calculations.

The first 1954 normal modes up to 300 cm^{-1} were calculated in four stages, 0−100, 100−200, 200−250, 250−300 cm^{-1}. To converge the first 696 normal modes up to 100 cm^{-1} we used a 200-vector block starting with a random set of vectors. The procedure required 807 iterations and took ∼300 h of CPU time on a single 2.4 GHz processor. The other three stages were completed with 100-vector blocks. It was observed that the lowest root in each stage was always higher than the highest root of the previous stage, as is required by the variational principle. We are thus confident that no roots were missed in the procedure. Figure 3 shows the convergence profile of the lowest 10 normal modes in the later steps of diagonalization. The early steps of the algorithm, iterations 1−20, quickly remove the high frequency components from the guess vectors. The following iterations simply work to refine the strongly coupled vectors, and it may take hundreds of iterations to cleanly separate the true eigenstates. Thus, the initial guess is not as important as the size of the block (the bigger the block, the more efficient the convergence) or the preconditioning scheme. Reiher et al. investigated the effects of the approximate inverse of **K** in eq 5 and found encouraging results.[20] Their scheme can also be applied in the present calculations.

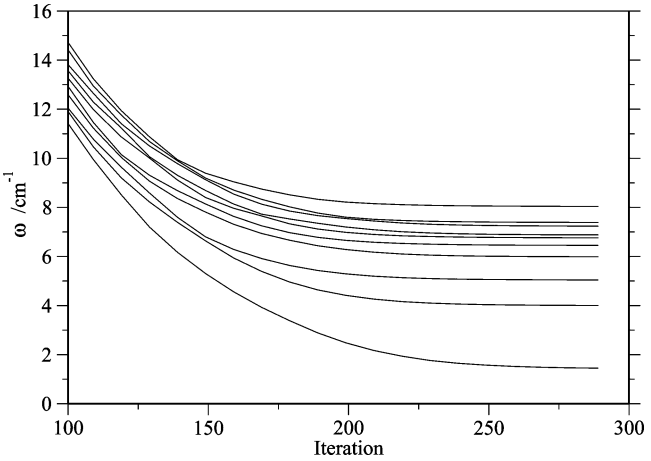

Figure 3. The convergence of the lowest 10 normal-mode frequencies of WT-bR. Note the configuration mixing occurring between 100 and 200 iterations, seen here as "avoided crossing". The nearly degenerate pairs (6,7) and (8,9) change character several times before iteration 200. The lowest root uncouples from the rest at early stages but converges very slowly.

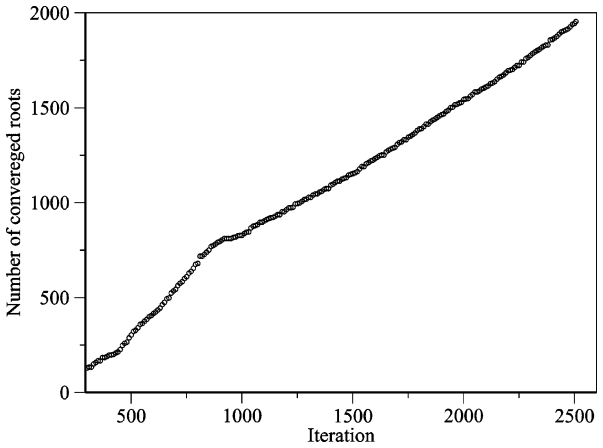

Figure 4. The number of converged normal-mode frequencies of WT-bR as a function of iterations. Note the crossover point at 807 iteration where the block size was reduced from 200 to 100.

Figure 4 demonstrates the dependence of the number of converged roots as a function of iterations. The lowest part of the spectrum that contains many delocalized vibrations is very difficult to converge. Note that it took 294 iterations to converge the first root, $\omega_1 = 1.442$ cm^{-1}. Overall, the first 123 modes converged in 300 iterations. The convergence curve as a function of iteration appears to be a superposition of two lines. The crossover point occurs at 807 iteration

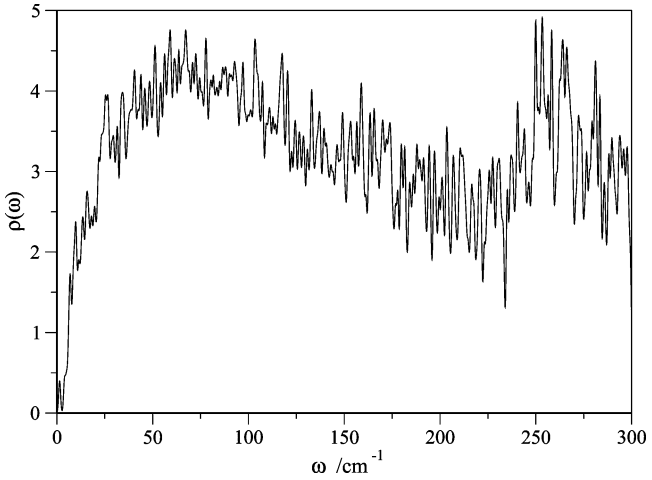

Figure 5. Unaveraged density of normal modes of WT-bR.

where the block size was changed from $L = 200$ to $L = 100$. The smaller block results in more iterations per root. Simple extrapolation can give an estimate of the computational cost required to obtain more roots, provided the density of states does not change rapidly.

A density of the normal modes of WT-bR up to 300 cm^{-1} is plotted in Figure 5. The NM distribution has been represented as a sum of Gaussians with a width 0.5 cm^{-1}. The density of the states is very broad and increasing up to 75 cm^{-1}, similar to experimental measurements.[61] Above 75 cm^{-1} the density of the states slowly decreases and then goes up again at 250 cm^{-1}. Experimental measurements of infrared absorbance of bR in solution show similar behavior.[11]

Among many useful properties, normal modes can be used to determine the role of collective motions in the dynamics of the system. The participation ratios have been used to characterize the degree of delocalization of the normal modes in liquid[67] and protein systems.[69,70] The participation ratios are defined as follows

$$R_I^a = \sum_j^{3N} (y_{Ij})^4 \tag{18}$$

$$R_I^r = \sum_l^{N_r} [\sum_j^{3N_l} (y_{Ij})^2]^2$$

where N_r is the number of residues, and N_l is the number of atoms in the lth residue. One can interpret $1/R_I^a$ as the number of degrees of freedom involved in the Ith mode and $1/R_I^r$ as the number of protein residues participating in that mode. If a mode is completely localized, only one of the eigenvector coefficients will be nonzero and $1/R_I^a$ will be equal to unity. On the other hand, if a mode is completely delocalized, each degree of freedom will be equally involved in that mode and $1/R_I^a$ will be equal to $3N$.

Table 1 shows the lowest 20 normal-mode frequencies of WT-bR up to 10 cm^{-1} with the corresponding residual norms (eq 6), quantum lifetimes (eq 16), and participation ratios (eq 18). Low-frequency modes are typically delocalized throughout the protein and involve mainly collective movements of residues. Most of the normal modes of WT-bR up to 10 cm^{-1} are delocalized, with $1/R_I^a > 200$. However, the lowest normal mode $\omega_1 = 1.442$ cm^{-1} is almost completely localized on the loop that connects helices B and C (Figure 6), and the participation ratio suggests involvement of only 5 residues (residues 68−72) GLY-GLY-GLU-GLN-ASN.

Table 1. Lowest Frequencies in cm^{-1} of WT-bR with the Associated Residual Errors, Quantum Lifetime in ps, and the Inverse Participation Ratios Defined in Eq 18

I	ω_I	$\|r_I\|$	τ_I(0 K)	$1/R_I^a$	$1/R_I^r$
1	1.442	0.18156E-8	0.16	39	5
2	4.003	0.13395E-8	11.0	1211	99
3	5.042	0.12619E-8	5.0	894	89
4	5.988	0.15719E-8	8.6	993	86
5	6.452	0.12818E-8	15.1	306	24
6	6.760	0.14046E-8	11.5	914	75
7	6.877	0.18801E-8	6.8	382	37
8	7.234	0.19270E-8	6.8	284	29
9	7.388	0.13283E-8	9.5	79	8
10	8.040	0.16267E-8	21.4	857	64
11	8.434	0.11833E-8	6.8	600	56
12	8.530	0.16593E-8	20.0	807	50
13	8.883	0.16471E-8	4.1	388	42
14	9.088	0.21947E-8	22.2	238	21
15	9.281	0.15329E-8	18.5	325	31
16	9.737	0.18148E-8	24.5	236	26
17	9.778	0.13752E-8	12.6	353	30
18	9.959	0.14946E-8	24.4	817	68
19	10.111	0.16286E-8	15.3	157	14
20	10.190	0.16805E-8	17.4	900	76

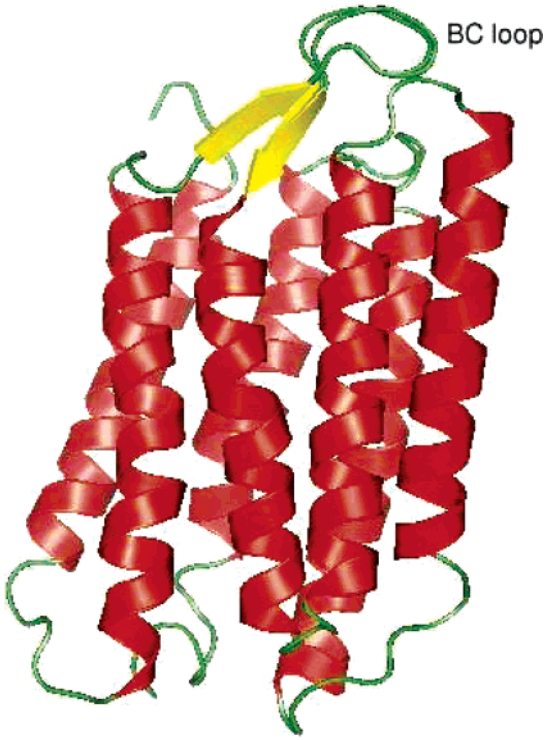

Figure 6. The 1.442 cm^{-1} mode of WT-bR represented as two superimposed structures: the equilibrium and the slightly displaced structure with $\delta E = 3.6$ cm^{-1} along the normal mode vector. The largest displacements occur in the BC loop in the extracellular part of the protein. The figure was created with PyMOL.[68]

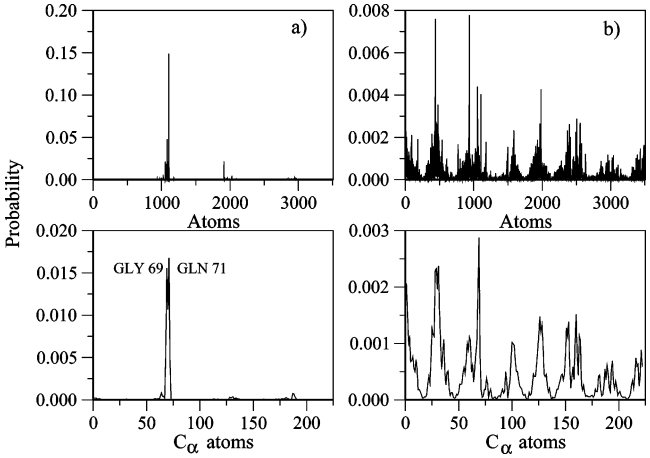

Figure 7. Squared amplitudes summed over the three Cartesian directions for all atoms (upper panels) and C_α atoms (bottom panels) for the lowest two normal modes (a) $\omega_1 = 1.442$ cm^{-1} and (b) $\omega_2 = 4.003$ cm^{-1}. The lowest normal mode is completely localized on the BC loop, while the second mode represents typical collective motion.

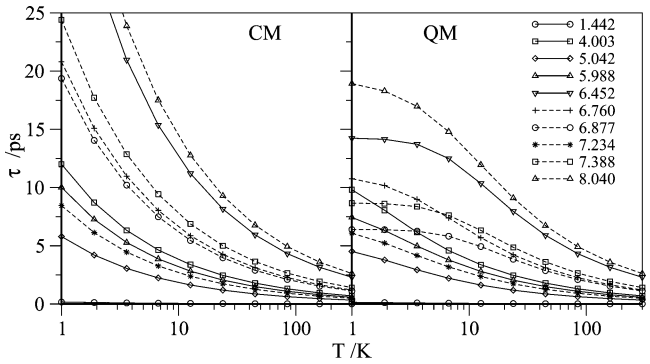

Figure 8. Temperature dependence of lifetimes up to 300 K of several low-frequency modes of WT-bR. The lifetime calculations were done using formulas 16 (for QM results) and 17 (for CM results). The summations included the states up to 40 cm^{-1}, a total of 200 states. The horizontal scale is logarithm base of 10.

For comparison, we plot displacements of all atoms and C_α's of the two lowest normal modes in Figure 7. The largest displacements correspond to C_α's of GLY-69 and GLN-71 residues. We noted that the C_α's displacements are much smaller than displacements of the protein side chains. The greater flexibility of the interhelical loops was predicted in molecular dynamics studies.[71,72]

The lifetime of the highly localized lowest frequency mode, $\tau_1 \approx 161$ fs, is an order of magnitude shorter than the lifetime of the other modes, pointing to its spatial instability, i.e., propensity to jump to another minimum. Thermal stability of the normal modes is depicted in Figure 8 where we compare quantum and classical calculations. As expected, the lower frequency modes reach the classical limit ($1/k_BT \rightarrow 0$) faster than the higher frequency ones, and, already at 10 K, the classical results for all the frequencies up to 10 cm^{-1} are similar to the quantum ones. It is interesting to note that some modes destabilize much quicker than others with increasing temperature. For example, $\omega_2 = 4.003$ cm^{-1} which corresponds to the collective motion (see Figure 7b)

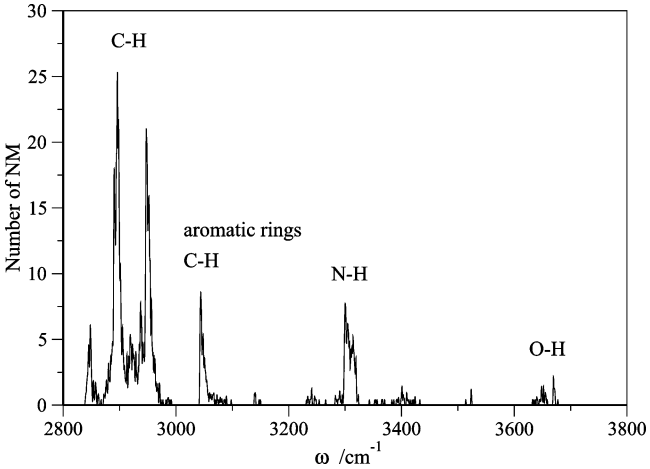

Figure 9. High-frequency vibrations of WT-bR.

has a sharply decreasing lifetime curve, crossing two states. On the other hand, $\omega_7 = 6.877$ cm^{-1} has a flat lifetime curve up to 10 K.

The upper extreme of the spectrum between 2840 and 3680 cm^{-1} was also obtained using the technique mentioned in section 2. For the dominant spectral features the atomic motion was analyzed, and the peaks were assigned (Figure 9). The spectrum contains localized A−H vibrations (where A = C, N, O) that converged more rapidly than the collective modes. Using a 100 vector block, it took 700 iterations to converge all the 1782 high frequency modes. The sliding block procedure clearly identified the gap in the density of states of WT-bR. The modes $\omega_{8721} = 1751.8$ cm^{-1} localized on the E helix (C−C stretch of the TRP-134 side chain) and $\omega_{8722} = 2839.3$ cm^{-1} localized on the BC loop (C−H stretch of the MET-64 side chain) represent the left and right sides of the gap in the spectrum.

To briefly address the usefulness of sparse matrix diagonalization approaches and possibly shed light on the origin of the localized lowest frequency mode, we performed diagonalization using a cutoff scheme for the long-range interactions. All the nonbonded interactions were truncated at several values, and the lowest few roots were converged for each value of the cutoff radius, r_c. Truncation of the nonbonded interactions is equivalent to the removal of small off-diagonal Hessian elements based on a threshold. The resulting eigenvalues are approximate, although the errors of such calculations are rarely reported. Figure 10 shows the dependence of the first three frequencies on the cutoff radius. The frequencies are barely perturbed for $r_c > 25$ Å indicating that there are no dynamically significant interactions beyond 25 Å. However, as the cutoff radius is made smaller, the lowest mode undergoes substantial variations in frequency, and in the range $12 < r_c < 22$ Å it becomes unstable, while the excited states remain roughly the same. If the nonbonded forces are removed for all distances less than 10−11 Å, the modes lose their identity, as seen by the plunging curves in the figure, and the protein is possibly distorted to a nearby structure (a local minimum). The participation ratios of the lowest mode are also quite sensitive to the interaction radius. At 15 Å, for example, $1/R_I$ is about 84 and still bears characteristics of a localized mode, but at 11 Å, R_I is 1100, the signature of a typical collective mode.

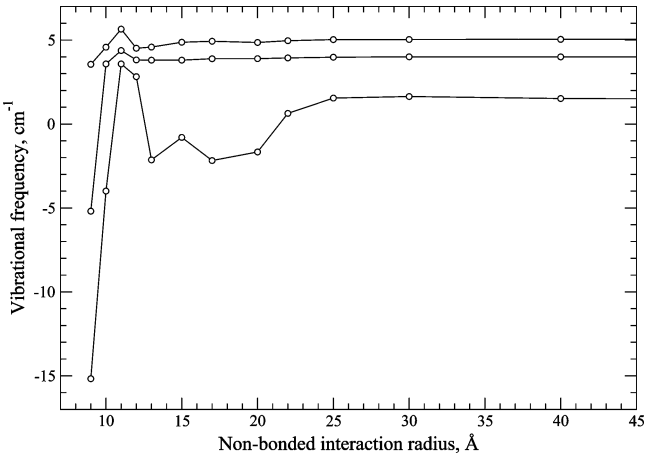

Figure 10. Dependence of the lowest three modes on the nonbonded interaction radius. The negative values on the vertical axis designate imaginary frequencies.

4. Concluding Remarks

The gradient based iterative diagonalization method presented here is designed specifically to treat large biomolecules on the all-atom basis. The method is CPU-bound, rather than memory-bound, and its scaling properties are akin to molecular dynamics simulations. Each iteration L Hessian-vector products ($2L$ gradients) are computed. In sequential calculations the gradient evaluations comprise the main bottleneck, although it is clear that massive parallelization (for large L) is almost trivial since the L Hessian-vector products are unrelated to each other.

Because the iterative subspace is nonexpanding, only the $3L$ vectors and their $3L$ Hessian products need to be stored in memory, resulting in a total storage of $18LN$ elements for a molecule with N atoms. In double precision, the rule of thumb for the memory is 144 MB for a 100-vector block per 10^4 atoms. Thus, all-atom calculations for systems with up to 10^6 atoms are not unrealistic, and it is possible to converge the entire spectrum while storing only the $3L$ vectors and their $3L$ Hessian products in memory.

Calculations are presented for a moderate size protein, WT-bR (3503 protein atoms, 222 residues), in gas phase. Analysis of the results points to two observations: (i) the existence of noncollective, localized low-frequency modes in proteins, also found in the recent calculations of Cui et al.[73] and (ii) the importance of the long-range electrostatic and van der Waals interactions. In conventional macromolecular simulations, to speed up the calculation, cutoff schemes[74] are applied to all nonbonded interactions. (For example, in WT-bR the nonbonded interactions cutoff at 20 and 13 Å reduced the effort to compute the gradient by three and four times, respectively.) Although the cutoff approximation may not always cause severe problems, it should be used with caution, especially if the simulation involves charge transfer. The calculations presented here have revealed that long-range forces acting up to 25 Å can destabilize some of the low-frequency modes. It is thus conceivable that the NMA methods that use sparse matrix techniques may not properly capture the vibrational dynamics by simply discarding the many small matrix elements. More numerical tests are necessary to better understand the potential dangers of using the sparse Hessian approaches for macromolecules.

Acknowledgment. We thank the National Science Foundation for the support, grant No. CHE-0446527.

References

(1) Wilson, E. B.; Decius, J. C.; Cross, P. C. *Molecular Vibrations*; McGraw-Hill: New York, 1955.

(2) Herzberg, G. *Molecular Spectra and Molecular Structure. II. Infrared and Raman Spectra of Polyatomic Molecules*; Van Nostrand: New York, 1945.

(3) *Normal mode analysis: Theory and applications to biological and chemical systems*; Cui, Q., Bahar, I., Eds.; CRC Press: 2005.

(4) Brooks, B. R.; Janežič, D.; Karplus, M. *J. Comput. Chem.* **1995**, *16*, 1522−1542.

(5) Janežič, D.; Brooks, B. R. *J. Comput. Chem.* **1995**, *12*, 1543−1553.

(6) Marques, O. A.; Sanejouand, Y.-H. *Proteins* **1995**, *23*, 557−560.

(7) Tama, F.; Sanejouand, Y.-H. *Protein Eng.* **2001**, *14*, 1−6.

(8) Durand, P.; Trinquier, G.; Sanejouand, Y.-H. *Biopolymers* **1994**, *34*, 759−771.

(9) Austin, R. H.; Hong, M. K.; Moser, C.; Plombon, J. *Chem. Phys.* **1991**, *158*, 473−486.

(10) Beratan, D. N.; Betts, J. N.; Onuchic, J. N. *J. Phys. Chem.* **1992**, *96*, 2852−2855.

(11) Xie, A.; Van der Meer, A. F. G.; Austin, R. H. *Phys. Rev. Lett.* **2002**, *88*, 018102-1−018102-4.

(12) Noid, D. W.; Fukui, K.; Sumpter, B. G.; Yang, C.; Tuzun, R. E. *Chem. Phys. Lett.* **2000**, *316*, 285−296.

(13) Fukui, K.; Sumpter, B. G.; Noid, D. W.; Yang, C.; Tuzun, R. E. *Comput. Theor. Polym. Sci.* **2001**, *11*, 191−196.

(14) Fukui, K.; Sumpter, B. G.; Noid, D. W.; Yang, C.; Tuzun, R. E. *J. Phys. Chem. B* **2000**, *104*, 526−531.

(15) Noid, D. W. private communication.

(16) Filippone, F.; Parrinello, M. *Chem. Phys. Lett.* **2001**, *345*, 179−182.

(17) Filippone, F.; Meloni, S.; Parrinello, M. *J. Chem. Phys.* **2001**, *115*, 636−642.

(18) Anglada, J. P.; Besalù E.; Bofill, J. M.; Rubio, J. *J. Math. Chem.* **1999**, *25*, 85−92.

(19) Prat-Resina, X.; Garcia-Viloca, M.; Monard, G.; González A.; Lluch, J. M.; Bofill, J. M.; Anglada, J. M. *Theor. Chem. Acc.* **2002**, *107*, 147−153.

(20) Reiher, M.; Neugebauer, J. *J. Chem. Phys.* **2003**, *118*, 1634−1641.

(21) Reiher, M.; Neugebauer, J. *Phys. Chem. Chem. Phys.* **2004**, *6*, 4621−4629.

(22) Neugebauer, J.; Reiher, M. *J. Comput. Chem.* **2004**, *25*, 587−597.

(23) Neugebauer, J.; Reiher, M. *J. Phys. Chem. A* **2004**, *108*, 2053−2061.

(24) Kaledin, A. L. *J. Chem. Phys.* **2005**, *122*, 184106-1−184106-7.

(25) Gerratt, J.; Mills, I. M. *J. Chem. Phys.* **1968**, *49*, 1719−1729.

(26) Pick, R. M.; Cohen, M. H.; Martin, R. M. *Phys. Rev. B* **1970**, *1*, 910.

(27) DeCicco, P. D.; Johnson, F. A. *Proc. R. Soc. A* **1969**, *310*, 111−119.

(28) Baroni, S.; Giannozzi, P.; Testa, A. *Phys. Rev. Lett.* **1987**, *59*, 2662.

(29) Gonze, X.; Vigneron, J.-P. *Phys. Rev. B* **1989**, *39*, 13120−13128.

(30) Davidson, E. R. *J. Comput. Phys.* **1975**, *17*, 87.

(31) Murray, C. W.; Racine, S. C.; Davidson, E. R. *J. Comput. Phys.* **1992**, *103*, 382−389.

(32) Leininger, M. L.; Sherrill, C. D.; Allen, W. D.; Schaefer, H. F., III *J. Comput. Chem.* **2001**, *22*, 1574−1589.

(33) Liu, B. *Numerical Algorithms in Chemistry: Algebraic Methods*; Moler, C., Shavitt, I., Eds.; LBL-8158; Lawrence Berkeley Laboratory: Berkeley, CA, 1978.

(34) Van Lenthe, J. H.; Pulay, P. *J. Comput. Chem.* **1990**, *11*, 1164−1168.

(35) Knyazev, A. V. *Electron. Trans. Num. Anal.* **1998**, *7*, 104−123.

(36) Knyazev, A. V. *Int. Ser. Numer. Math.* **1991**, *96*, 143−154.

(37) Knyazev, A. V. *SIAM J. Sci. Comput.* **2001**, *23*, 517−541.

(38) Saad, Y. *Numerical methods for large eigenvalue problems*; Manchester University Press: Halsted Press: Wiley: 1992.

(39) Lanczos, C. *J. Res. Nat. Bur. Standards* **1950**, *45*, 255−282.

(40) Sleijpen, G. L. G.; Van der Vorst, H. A. *SIAM Rev.* **2000**, *42*, 267−29.

(41) Lehoucq, R.; Sorensen, D. *SIAM J. Mater. Anal. Appl.* **1996**, *8*, 789−821.

(42) Lehoucq, R. B.; Sorensen, D. C.; Yang, C. *ARPACK Users' Guide: Solution of Large-Scale Eigenvalue Problems with Implicitly Restarted Arnoldi Methods*; SIAM: Philadelphia, PA, 1998.

(43) Anglada, J. M.; Besalù E.; Bofill, J. M. *Theor. Chem. Acc.* **1999**, *103*, 163−166.

(44) Bofill, J. M.; Moreira, I. D. P. R.; Anglada, J. M.; Illas, F. *J. Comput. Chem.* **2000**, *21*, 1375−1386.

(45) Maradudin, A. A.; Fein, A. E. *Phys. Rev.* **1962**, *128*, 2589−2608.

(46) Yu, X.; Leitner, D. M. *J. Phys. Chem. B* **2003**, *107*, 1698−1707.

(47) Fujisaki, H.; Bu, L.; Straub, J. E. *Adv. Chem. Phys.* **2005**, *130*, 179−203.

(48) Ponder, J. TINKER Software Tools for Molecular Design, Version 4.2, Washington University School of Medicine, June 2004, available from http:/dasher.wustl.edu/tinker.

(49) Neidigh, J. W.; Fesinmeyer, R. M.; Andersen, N. H. *Nature Struct. Biol.* **2002**, *9*, 425−430.

(50) Cheatham, T. E., III; Cieplak, P.; Kollman, P. A. *J. Biomol. Struct. Dyn.* **1999**, *16*, 845−862.

(51) Cornell, W. D.; Cieplak, P.; Bayly, C. I.; Gould, I. R.; Merz, K. M., Jr.; Ferguson, D. M.; Spellmeyer, D. C.; Fox, T.; Caldwell, J. W.; Kollman, P. A. *J. Am. Chem. Soc.* **1995**, *117*, 5179−5197.

(52) Lanyi, J. K. *Int. Rev. Cytol.* **1999**, *187*, 161−202.

(53) Ben-Nun, M.; Molnar, F.; Lu, H.; Phillips, J. C.; Martinez, T. J.; Schulten, K. *Faraday Discuss.* **1998**, *110*, 447−462.

(54) Ferrand, M.; Dianoux, A. J.; Petry, W.; Zaccai, G. *Proc. Natl. Acad. Sci. U.S.A.* **1993**, *90*, 9668−9672.

(55) Humphrey, W.; Xu, D.; Sheves, M.; Schulten, K. *J. Phys. Chem.* **1995**, *99*, 14549−14560.

(56) Xu, D.; Martin, C.; Schulten. K. *Biophys. J.* **1996**, *70*, 453−460.

(57) Xu, D.; Sheves, M.; Schulten, K. *Biophys. J.* **1995**, *69*, 2745−2760.

(58) Roux, B.; Nina, M.; Pomes, R.; Smith, J. C. *Biophys. J.* **1996**, *71*, 670−681.

(59) Ferrand, M.; Zaccai, G.; Nina, M.; Smith, J. C.; Etchebest, C.; Roux, B. *FEBS. Lett.* **1993**, *327*, 256−260.

(60) Zaccai, G. *Science* **2000**, *288*, 1604−1607.

(61) Whitmire, S. E.; Wolpert, D.; Markelz, A. G.; Hillbrecht, J. R.; Galan, J.; Birge, R. R. *Biophys. J.* **2003**, *85*, 1269−1277.

(62) Mouawad, L.; Perahia, D. *Biopolymers* **1996**, *33*, 599−611.

(63) Alexiev, U.; Mollaaghababa, R.; Khorana, H. G.; Heyn, M. P. *J. Biol. Chem.* **2000**, *275*, 13431−13440.

(64) Luecke, H.; Schobert, B.; Richter, H. T.; Cartailler, J. P.; Lanyi, J. K. *J. Mol. Biol.* **1999**, *291*, 899−911.

(65) MacKerell, A. D., Jr.; Bashford, D.; Bellott, M.; Dunbrack, R. L., Jr.; Evanseck, J. D.; Field, M. J.; Fischer, S.; Gao, J.; Guo, H.; Ha, S.; Joseph-McCarthy, D.; Kuchnir, L.; Kuczera, K.; Lau, F. T. K.; Mattos, C.; Michnick, S.; Ngo, T.; Nguyen, D. T.; Prodhom, B.; Reiher, W. E., III; Roux, B.; Schlenkrich, M.; Smith, J. C.; Stote, R.; Straub, J.; Watanabe, M.; Wiorkiewicz-Kuczera, J.; Yin, D.; Karplus, M. *J. Phys. Chem. B* **1998**, *102*, 3586−3616.

(66) Foloppe, N.; MacKerell, A. D., Jr. *J. Comput. Chem.* **2000**, *21*, 86−104.

(67) Cho, M.; Fleming, G. R.; Saito, S.; Ohmine, I.; Stratt, R. M. *J. Chem. Phys.* **1994**, *100*, 6672−6683.

(68) DeLano, W. L. The PyMOL Molecular Graphics System, DeLano Scientific LLC, San Carlos, CA. http://www.pymol.org.

(69) Sagnella, D. E.; Straub, J. E. *Biophys. J.* **1999**, *77*, 70−84.

(70) Bu, L.; Straub, J. E. *Biophys. J.* **2003**, *85*, 1429−1439.

(71) Rajamani, R.; Gao, J. *J. Comput. Chem.* **2002**, *23*, 96−104.

(72) Jang, H.; Crozier, P. S.; Stevens, M. J.; Woolf, T. B. *Biophys. J.* **2004**, *87*, 129−145.

(73) Cui, Q.; Li, G.; Ma, J.; Karplus. M. *J. Mol. Biol.* **2004**, *340*, 345−372.

(74) Steinbach, P. J.; Brooks, B. R. *J. Comput. Chem.* **1994**, *15*, 667−683.

CT050161Z